RSC Advances

PAPER

View Article Online
View Journal | View Issue

Cite this: *RSC Adv.*, 2019, **9**, 29149

Enantiomeric helical TiO_2 nanofibers modulate different peptide assemblies and subsequent cellular behaviors†

Xu Jie,‡[a] Deng Xu‡[b] and Weili Wei *[a]

Received 21st June 2019
Accepted 11th September 2019

DOI: 10.1039/c9ra04660g

rsc.li/rsc-advances

The effect of the morphological chirality of inorganic TiO_2 nanofibers on peptide assembly and cellular behaviors was investigated. Model peptide insulin maintains its native structure and served as a growth factor for promoting proliferation and differentiation of PC12 cells on the surface of right-handed TiO_2. In contrast, insulin forms amyloid fibrils and loses its bioactivity on the left-handed TiO_2.

Homochirality is one of the hallmarks of biomolecules such as the amino acids, sugars, and proteins that are the building blocks of life on earth.[1] Enantioselective chemistry on chiral inorganic crystalline surfaces makes a significant contribution to the homochirality of biomolecules.[2] From prebiotic organic molecule assemblages to the asymmetric biochemical behavior of biomolecules, the chemical interactions between inorganic crystalline surfaces and aqueous species contribute to the Earth's complexity and the geochemical origins and evolution of life.[3] Although research has been reported that focused on the adsorption[4] and catalysis[5] between small molecules (*e.g.*, amino acids) and chiral inorganic crystalline surfaces, the systematic inspection of the interaction between chiral inorganic surfaces and biomacromolecules (*e.g.*, protein) and the subsequent amplified effects on living cells has, as yet, hardly been explored.

The asymmetry of crystals provides the apparent chirality for natural minerals such as calcite single crystals and quartz which predate chiral organic molecules on Earth.[1,6] Chiral inorganic surfaces have been broadly used in phenomenological investigations and fundamental studies owing to their biocompatibility, physicochemical stability and well-organized arrangement of asymmetrical crystalline structures.[7,8] These precious features guarantee the intrinsic chirality can be retained even under harsh conditions such as high temperatures[9] and extreme acid or base environments.[10] In recent decades, titanium dioxide (TiO_2) has been widely used in tissue reconstruction, drug delivery and biosensing owing to its excellent biocompatibility, plasticity and chemical stability.[11,12] For instance, TiO_2 scaffolds or surfaces have been shown to enhance osteoblast adhesion, proliferation, and differentiation.[13,14] Therefore, it is of great significance to develop a chiral TiO_2 based inorganic surface that could open up a new frontier in our understanding and exploiting chiral morphology for biomacromolecules and even biological tissues and organs.

Enantiomeric left- and right-handed TiO_2 nanofibers (namely L- and R-TiO_2, respectively) were synthesized according to a previously reported method (see the ESI for details†).[15] Antipodal lipid–TiO_2 hybrids were formed by using a *N*-stearoyl-L/D-glutamic acid (C_{18}-L/D-Glu) lipid as the chiral template and titanium diisopropoxide bis(acetylacetonate) as the titanium source. L- and R-TiO_2 were obtained by removing the organic lipids through calcination. Scanning electron microscopy (SEM) images revealed that the TiO_2 nanofibers which were prepared with C_{18}-L-Glu were entirely left-handed double-helical structures (L-TiO_2, Fig. 1a). The average length and width of a single

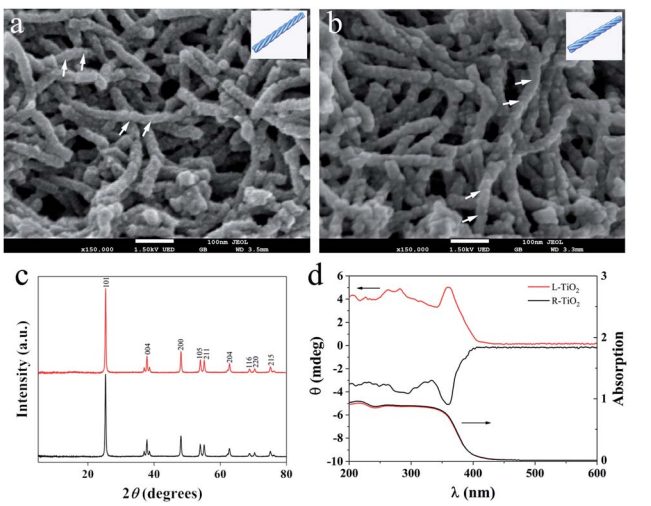

Fig. 1 (a) and (b) SEM images of the helical L- and R-TiO_2 nanofibers and corresponding schematic diagrams of the double-helical structures (insert). X-ray diffraction patterns (c), DRUV-Vis and DRCD spectra (d) of the L- and R-TiO_2 nanofibers.

[a]*School of Pharmaceutical Sciences and Innovative Drug Research Centre, Chongqing University, Chongqing 401331, China. E-mail: wlwei@cqu.edu.cn*

[b]*Chongqing Institute for Food and Drug Control, Chongqing 401121, China*

† Electronic supplementary information (ESI) available. See DOI: 10.1039/c9ra04660g

‡ These authors contributed equally to this work.

L-TiO_2 nanofiber was *ca.* 200 and 30 nm, respectively. Compared with L-TiO_2, the template molecule C_{18}-D-Glu endows R-TiO_2 with a mirror image profile with analogical size and quality (Fig. 1b). The transmission electron microscopy (TEM) images suggest that the TiO_2 nanofibers are composed of stacked small single crystals with an average size of 25 nm along the long axis of the fiber (see Fig. S1, ESI†). As demonstrated in Fig. 1c, the crystallographic structures of the L- and R-TiO_2 were confirmed using X-ray diffraction (XRD). Both of their diffraction peaks were indexed to the anatase (JCPDS card no. 21-1272) phase of TiO_2 without any indication of other crystalline impurities or by-products.

The chiral configuration and helical stacking of the TiO_2 nanofibers endowed the materials with optical activity (OA), which is demonstrated in Fig. 1d. The diffuse-reflection ultraviolet-visible (DRUV-Vis) spectra of the chiral TiO_2 nanofibers exhibits a broad absorption band in the range of 200–400 nm, and these bands are attributed to the electronic transition from the valence band to the conduction band.[15] The L- and R-TiO_2 exhibit obvious mirror-image diffuse-reflection circular dichroism (DRCD) signals with a peak at *ca.* 360 nm, which indicated that the OA of the chiral TiO_2 nanofibers is primarily a reflection of the intrinsic electronic structure. The optically active TiO_2 nanofibers selectively reflect left- or right-handed circularly polarized light in the ultraviolet absorption region through a vicinal effect of helically arranged TiO_2 crystals. These results indicated that the helical templates were successfully transcribed into the microscopic assembly of TiO_2, thus forming the enantiomeric TiO_2 nanofibers. The morphological and optical properties of L- and R-TiO_2 were the same as those reported previously.[15]

L- or R-TiO_2 were immobilized on the glass substrates[16] to form enantiomeric inorganic TiO_2 surfaces (denoted as L-surface and R-surface, respectively, see Scheme S1, ESI†). Then, the effect of the inorganic morphological chirality on the behavior of the peptide adsorption and assembly was investigated. Insulin controls the glucose metabolism and acts as a growth factor in mammals. It presents a α-helical structure in the native conformation, and the amyloidosis of insulin is commonly observed at the site of repeated insulin injections in patients with type II diabetes as well as in clinical formulations.[17] Previously, we reported that insulin can recognise the surface chirality of monolayer tartaric acids.[18] Herein, insulin was used as the model peptide to gain further insight into the interaction between the chirality of the inorganic materials and biomacromolecules.

The conformation of adsorbed insulin on TiO_2 chiral surfaces was first investigated using fluorescence microscopy *via* specific staining of the adsorbed insulin with thioflavine-T (ThT), a dye which is widely used for visualizing β-sheet-rich amyloid fibrils.[19] As shown in Fig. 2a, after 24 h of incubating insulin with L-surface, a cloud-like image with ambiguous edges and an intense brightness of ThT fluorescence was observed, proving the insulin existed as β-sheet-rich fibrils. In contrast, only a weak ThT fluorescence with several weak dots was observed on the R-surface (Fig. 2b).

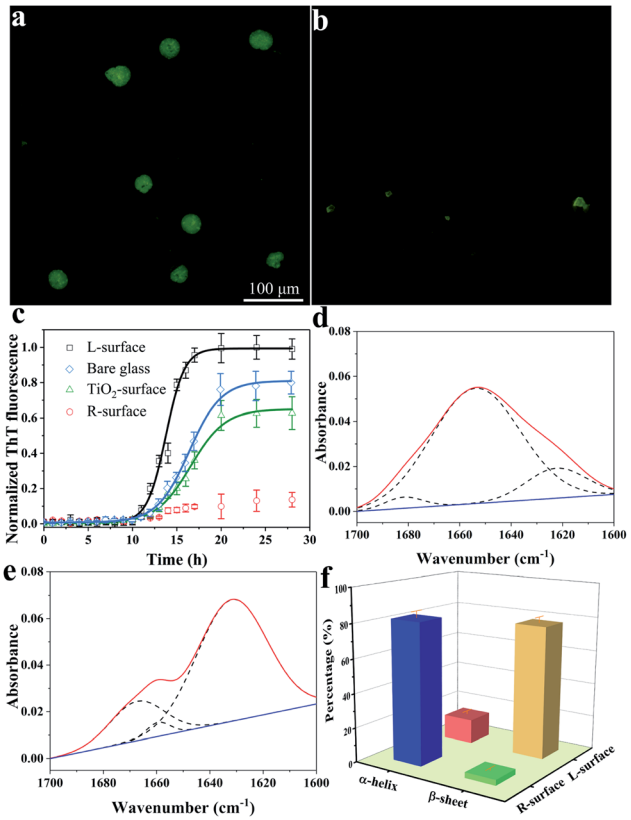

Fig. 2 Fluorescence microscopy images of L-surface (a) and R-surface (b) adsorbed insulin using ThT staining, and time dependence curves of the fluorescence intensity on different surfaces (c). The amide I bands of the ATR-FTIR spectra with fitted component peaks on the R-surface (d) and L-surface (e). (f) Statistical percentage of α-helix and β-sheet structures of insulin on the R- and L-surfaces. Results are expressed as mean ± standard deviation of three independent experiments.

The fibrillation process of insulin follows a nucleated-growth mechanism which can be divided into a lag phase, rapid exponential growth period and a final equilibrium stage.[20] According to the time-dependent fluorescence variation curves (Fig. 2c), the fluorescence of the bare glass surface was exponentially increased and reached an equilibrium after a lag phase of 10 h. In comparison, insulin on the L-surface has a shorter exponential growth period and a higher maximum florescence intensity compared to bare glass. These phenomena suggest that the insulin was assembled and formed fibrils on both the bare glass and the L-surface, and the presence of the L-TiO_2 nanofibers accelerated this fibrillation process. On the contrary, only a weak ThT fluorescence was observed on the R-surface, indicating that the disorganized initial aggregates, which lacked a β-sheet structure owing to the left-helical structure of the TiO_2 nanofibers suppressed the initial nucleation of insulin.[18,21,22] In addition, an achiral TiO_2 nanofibers modified surface (TiO_2 surface) was prepared, the DRCD spectra proved the prepared TiO_2 nanofibers do not have chirality (see Fig. S2, ESI†), and the ThT assay demonstrated it has a longer exponential growth period and lower maximum florescence

compared to the L-surface. This result further demonstrated that the presence of chirality on the surface can affect the fibrillation process of insulin. The significant differences between the insulin assembly on the R- and L-surfaces was further confirmed by using atomic force microscopy (AFM). After long-term incubation of insulin, the short oligomers with heights within 6 nm were formed on the R-surfaces; in contrast, the fibroid insulin assemblies, which were micrometers long and had a mean height of 10.5 ± 0.6 nm were observed on the L-surfaces (see Fig. S3, ESI†). The results of the AFM imaging were in good agreement with the ThT fluorescence experiments. All of the above described results indicated that the differences in the chiral crystalline surface prominently affects the assembly behavior of insulin on the chiral surface.

The conformational transition from an α-helix to a β-sheet is the foundation for the formation of oligomers or further fibrillation.[23,24] To investigate the mechanism of insulin assembly on chiral TiO_2 surfaces, a series of trials were carried out. Firstly, attenuated total reflection Fourier-transform infrared (ATR-FTIR) was used to investigate the secondary structure of the R- or L-surface adsorbed insulin. As demonstrated in Fig. 2d and e, the R-surface absorbed insulin assemblies presented a maximum absorbance peak at 1654 cm^{-1} which was ascribed to the characteristic band of the α-helical structure of insulin. Nevertheless, an obvious main peak at 1632 cm^{-1} for the insulin assemblies on the L-surface was observed, which suggested that the protein exists in a β-sheet structure.[25] In addition, quantitative analysis of the FTIR spectra was carried out using deconvolution and curve-fitting (Fig. 2f), the results indicated that 82.2% of the insulin on the R-surface were α-helical structures and 14.4% were β-sheet structures. On the contrary, most of the insulin assemblies on the L-surface were β-sheet structures (77.6%), and only 3.1% were in the α-helical conformation. The results implied that the L-surface facilitated the conformation conversion from α-helical to β-sheet structures owing to the fibrillation of insulin. Nevertheless, the R-surface maintained the native α-helical structure of insulin.

To further inspect the reason for the different insulin assembly behaviors induced by chiral TiO_2, the adsorption kinetics of the monomers and oligomers on chiral inorganic surfaces were further investigated using a quartz crystal microbalance (QCM).

After successful decoration of dopamine (see Fig. S4, ESI†), the TiO_2 nanofibers were covalently anchored onto the Au electrode surface of the QCM resonators (see Scheme S2, ESI†).[26] The insulin monomers (Fig. S5a, ESI†) exhibited an obviously stronger adsorption on the R-surface compared to the L-surface, inducing a frequency change (ΔF) of quartz crystals at −9.1 and −5.2 Hz, corresponding to adsorption quantities of 160.8 and 91.9 ng cm^{-2}, respectively. This result was further verified by the microscale thermophoresis (MST) experiment, which demonstrated an obvious interaction between the R-TiO_2 and insulin monomers at pH 1.6 (see Fig. S6a, ESI†). On the other hand, there is no distinct interaction between the L-TiO_2 and insulin monomers (see Fig. S6b, ESI†). Interestingly, compared with the insulin monomer, insulin oligomers (Fig. S5b, ESI†) undergo much stronger adsorption on both the R- and L-surfaces. However, the adsorption quantities are inversed between the R- and L-surfaces in comparison to the insulin monomers. When the amount of adsorption of the oligomers reached saturation, the shifts in the resonant frequency (ΔF) of the R-surface and L-surface were −27.7 and −54.7 Hz, corresponding to adsorption quantities of 489.4 and 961.1 ng cm^{-2}, respectively. The interaction between the R-surface and insulin monomer is stronger as the insulin monomer is composed of L-amino acid residues, and had right-handed helical structures.[18] However, with the unfolding and subsequent formation of oligomers, the secondary structure of insulin changes and leads to the inverse chirality. As a result, a stronger interaction was observed between the chiral L-TiO_2 surface and insulin oligomers. All of the above results demonstrate that the R-TiO_2 inorganic surface inhibits insulin fibrillation, while the L-TiO_2 inorganic surface promotes this process.

The adhesion force between the chiral TiO_2 and insulin is generated by the bonding of amino acid residues in insulin and the O^- and OH^{2+} groups on the surface of TiO_2.[27] In addition, the different adsorption behaviors are mainly attributed to the steric interaction between the insulin and chiral TiO_2 surface. For instance, the helical arrangement of the nanoscale lattice planes of TiO_2 in the R-surface provides a right-handed helical structure, which strongly interacts with the same helical insulin monomer. Therefore, the R-surface leads the initial orientation of the insulin molecules and maintains the natural activity. On the contrary, the insulin monomers unfold partially and accumulate on the surface to form oligomer nuclei owing to the weaker interaction between the monomer insulin and L-surface. Then, the insulin oligomer was accumulated for further formation of multilayered fibrils owing to the strong interaction between the oligomer and L-surface.

Although TiO_2 exhibits superiority in biomedical devices and functional biomaterials,[11] the impact of chirality on tissues or even cells has scarcely been studied. Inspired by the distinct impact on the insulin adsorption behaviors, a further investigation of the R- and L-TiO_2 surface adsorbed insulin as growth and neuronal differentiation factors for cell proliferation and differentiation was carried out. Here, typical neuron cell line PC12 cells were employed as a model and the cells were stained with fluorescent dye before microscopy imaging. After an initial 6 h culture, the PC12 cells were successfully adhered onto both the insulin-adsorbed L- and R-surfaces (Fig. 3a and b), and the cell density on the R- and L-surfaces was found to be 7900 ± 500 and 7600 ± 600 cm^{-2}, respectively (Fig. 3g). The results suggest that different insulin assemblies and conformations have little effect on PC12 adhesion.

Interestingly, after adhesion of PC12 cells on insulin-adsorbed surfaces and further culturing for 72 h, a contrasting difference in the cellular proliferation and differentiation was observed. On insulin-adsorbed R-surfaces, the PC12 cells proliferated rapidly and the population increased more than four times compared to the initial state (Fig. 3c). However, reduced cell growth was observed on top of the insulin-adsorbed L-surface (Fig. 3d). In order to inspect the effect of

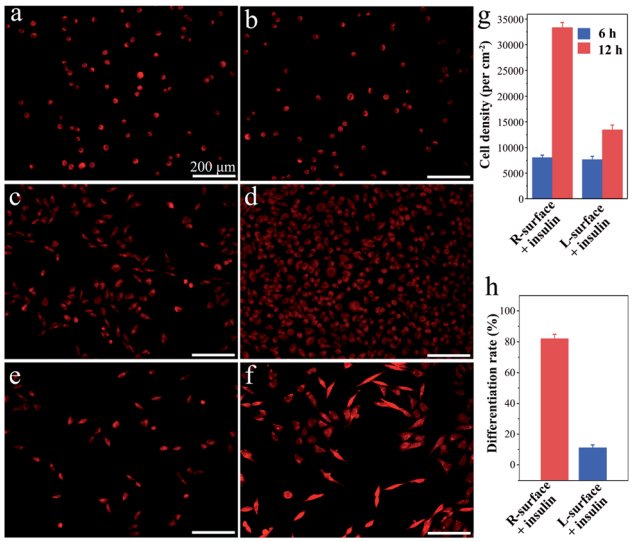

Fig. 3 Cellular responses of PC12 at the insulin absorbed chiral surfaces. The adhesion number of PC12 at (a) the insulin-adsorbed L-surface, and (b) the insulin-adsorbed R-surface. The fluorescence microscopy images were taken after PC12 were seeded for 6 h. (c) and (d) Fluorescence microscopy images of PC12 cells proliferated at the insulin-adsorbed L- and R-surfaces after culturing for 72 h, respectively. (e) and (f) Fluorescence microscopy images of PC12 cells differentiated at the insulin-adsorbed L- and R-surfaces after culturing for 72 h, respectively. (g) Estimation of the PC12 density. The seeding PC12 concentration was about 8000 cells per mL. (h) Statistics for PC12 differentiation after culturing for 72 h. The seeding PC12 concentration was about 4000 cells per mL.

the insulin-adsorbed chiral TiO_2 surface on cell differentiation, a reduced amount of initial PC12 cells were grown and cultured for 72 h. The obvious differentiation characteristics, such as the outgrowth of neurites and the formation of branching trees on the PC12 cells, were observed on the insulin-adsorbed R-surfaces (Fig. 3f). Nevertheless, compared with the insulin-adsorbed R-surfaces, less cells were differentiated on the insulin-adsorbed L-surfaces (Fig. 3e). Furthermore, the calculated differentiation rates of PC12 cells on the insulin-adsorbed R- and L-surfaces were 81.8 ± 3.2% and 11.0 ± 2.4%, respectively (Fig. 3h). According to above mentioned results, this was probably due to the insulin maintaining the native helical structure and retaining the bioactivity after being adsorbed on the surface of R-TiO_2, then as the growth and differentiation factors of insulin interacted with the receptors which were expressed on the plasma membrane surfaces, promotion of the growth and differentiation of the PC12 cells followed. However, the highly aggregated insulin fibrils were insoluble and lost their bioactivity on the surface of L-TiO_2.[28] All of these results proved that the inorganic TiO_2 chirality can strongly influence the protein assembly and its bioactivity, and further determines the fate of the cells, such as proliferation and differentiation.

In summary, two enantiomeric TiO_2 nanofibers were successful prepared. Then, the peptide assembly and subsequent cellular behaviors on L- and R-TiO_2 surfaces were investigated. This report indicated that the insulin assembling on the surface chiral TiO_2 nanofibers was different owing to the distinct interaction between the different topographic structures of the surfaces and the chiral structures of the proteins. Insulin maintains its native structure and served as a growth factor for promoting proliferation and differentiation of PC12 cells on the R-surface. In contrast, on the L-surfaces, insulin forms amyloid fibrils and loses its bioactivity. The interaction between the biomolecule and the chiral inorganic TiO_2 nanofiber surface studied here may provide new insights into developing biocompatible materials and understanding the origins of homochirality in nature.

Conflicts of interest

There are no conflicts to declare.

Acknowledgements

Financial support was provided by the Fundamental Research Funds for the Central Universities (No. 106112017CDJXSYY0001), and the National Natural Science Foundation of China (No. 21675016).

Notes and references

1 R. M. Hazen and D. S. Sholl, *Nat. Mater.*, 2003, **2**, 367.
2 A. Ben-Moshe, S. G. Wolf, M. B. Sadan, L. Houben, Z. Fan, A. O. Govorov and G. Markovich, *Nat. Commun.*, 2014, **5**, 4302.
3 R. M. Hazen and D. A. Sverjensky, *Cold Spring Harbor Perspect. Biol.*, 2010, **2**, a002162.
4 F. Zaera, *Chem. Soc. Rev.*, 2017, **46**, 7374.
5 T. Kawasaki, Y. Araki, K. Hatase, K. Suzuki, A. Matsumoto, T. Yokoi, Y. Kubota, T. Tatsumi and K. Soai, *Chem. Commun.*, 2015, **51**, 8742.
6 A. J. Gellman, Y. Huang, X. Feng, V. V. Pushkarev, B. Holsclaw and B. S. Mhatre, *J. Am. Chem. Soc.*, 2013, **135**, 19208.
7 C. A. Orme, A. Noy, A. Wierzbicki, M. T. Mcbride, M. Grantham, H. H. Teng, P. M. Dove and J. J. Deyoreo, *Nature*, 2001, **411**, 775.
8 B. Paredes, A. Widera, V. Murg, O. Mandel, S. Folling, I. Cirac, G. V. Shlyapnikov, T. W. Hansch and I. Bloch, *Nature*, 2004, **429**, 277.
9 H. Matsukizono and R.-H. Jin, *Angew. Chem., Int. Ed.*, 2012, **51**, 5862.
10 H. Matsukizono, H. Murada and R.-H. Jin, *Chem.–Eur. J.*, 2014, **20**, 1134.
11 S. Wu, Z. Weng, X. Liu, K. W. K. Yeung and P. K. Chu, *Adv. Funct. Mater.*, 2014, **24**, 5464.
12 Z. Fei Yin, L. Wu, H. Gui Yang and Y. Hua Su, *Phys. Chem. Chem. Phys.*, 2013, **15**, 4844.
13 X. Wang, R. A. Gittens, R. Song, R. Tannenbaum, R. Olivares-Navarrete, Z. Schwartz, H. Chen and B. D. Boyan, *Acta Biomater.*, 2012, **8**, 878.
14 D. S. Kommireddy, S. M. Sriram, Y. M. Lvov and D. K. Mills, *Biomaterials*, 2006, **27**, 4296.

15 S. Liu, L. Han, Y. Duan, S. Asahina, O. Terasaki, Y. Cao, B. Liu, L. Ma, J. Zhang and S. Che, *Nat. Commun.*, 2012, **3**, 1215.
16 J. Lee, K. Ha, Y. J. Lee and K. B. Yoon, *Adv. Mater.*, 2005, **17**, 837.
17 S. Okamura, Y. Hayashino, S. Kore-Eda and S. Tsujii, *Diabetes Care*, 2013, **36**, E200.
18 W. Wei, C. Xu, N. Gao, J. Ren and X. Qu, *Chem. Sci.*, 2014, **5**, 4367.
19 H. Levine, *Protein Sci.*, 1993, **2**, 404.
20 M. I. Smith, J. S. Sharp and C. J. Roberts, *Biophys. J.*, 2007, **93**, 2143.
21 L. Nielsen, R. Khurana, A. Coats, S. Frokjaer, J. Brange, S. Vyas, V. N. Uversky and A. L. Fink, *Biochemistry*, 2001, **40**, 6036.
22 S. H. Li, L. Y. Wang, C. C. Chusuei, V. M. Suarez, P. L. Blackwelder, M. Micic, J. Orbulescu and R. M. Leblanc, *Chem. Mater.*, 2015, **27**, 1764.
23 L. Fu, J. Liu and E. C. Y. Yan, *J. Am. Chem. Soc.*, 2011, **133**, 8094.
24 S. H. Li and R. M. Leblanc, *J. Phys. Chem. B*, 2014, **118**, 1181.
25 S. Mauri, M. Volk, S. Byard, H. Berchtold and H. Arnolds, *Langmuir*, 2015, **31**, 8892.
26 G. Qing, S. Zhao, Y. Xiong, Z. Lv, F. Jiang, Y. Liu, H. Chen, M. Zhang and T. Sun, *J. Am. Chem. Soc.*, 2014, **136**, 10736.
27 T. Hayashi, K.-I. Sano, K. Shiba, Y. Kumashiro, K. Iwahori, I. Yamashita and M. Hara, *Nano Lett.*, 2006, **6**, 515.
28 V. Novitskaya, O. V. Bocharova, I. Bronstein and I. V. Baskakov, *J. Biol. Chem.*, 2006, **281**, 13828.